Chapter 7

Nucleoside-dependent switching between active and passive unwinding in a nidovirus superfamily 1 RNA helicase

Aartjan J.W. te Velthuis[1,2], David Dulin[1], Danny D. Nedialkova[2#], Suzanne S. Hage[1], Eric J. Snijder[2], and Nynke H. Dekker[1]

[1] Department of Bionanoscience, Kavli Institute of Nanoscience, Delft University of Technology, Lorentzweg 1, 2628 CJ Delft, The Netherlands

[2] Department of Medical Microbiology, Molecular Virology Laboratory, Leiden University Medical Center, Albinusdreef 2, 2333 ZA Leiden, The Netherlands

Present address: Max Planck Institute for Molecular Biomedicine, Röntgenstraße 20, 48149 Münster, Germany

Abstract

RNA helicases are enzymes that are critically involved in the replication and transcription of RNA viruses. Although most RNA viruses encode so-called superfamily (SF) 1-type helicases, real-time kinetics data is currently only available on the SF2 type helicase NS3 of the hepatitis C virus. It is therefore unknown whether other viral RNA helicases use a comparable mechanism to couple ATP hydrolysis to the unwinding double-stranded helices or employ a different strategy to separate the strands. Here we present a single-molecule approach to study the unwinding activity of nsp10, the SFI type helicase of the nidovirus prototype equine arteritis virus (EAV). We find that nsp10 is able to use all four NTPs for the unwinding of double-stranded templates, but that the use of ATP, GTP and UTP results in high pause frequencies and a strong sequence-dependency, reminiscent of a passive unwinding mechanism. Strikingly, the hydrolysis of CTP makes the enzyme relatively insensitive to the local sequence and less prone to pausing. These results suggest that the mode of chemo-mechanical coupling during duplex unwinding is not a fixed parameter and dependent on the nucleotide present in the active site.

Introduction

RNA helicases are important agents in the metabolism of nucleic acid and play key roles in transcription, translation, and replication in eukaryotic cells, bacteria and both DNA and RNA viruses [372,373]. In addition, RNA helicases have been implicated in the expansion of viral positive-stranded RNA (+RNA) genomes from a few hundred bases to up to ~31 kilo bases [35,37] and are often strictly required during the RNA virus life cycle, which makes them valuable targets for antiviral therapy [276,372]. Phylogenetic analysis and biochemical studies have shown that particularly the superfamily (SF) 1-type helicase motifs are well-conserved among RNA viruses. Although this type of helicase domain is believed to be structurally and functionally different from other SF types [373,374,375], detailed knowledge of the unwinding dynamics of its RNA viral representatives is currently very limited and mostly based on extrapolation from the well-studied SF2 type helicase NS3 of the hepatitis C virus (HCV) [376,377,378,379].

SF1 type helicases are encoded by a variety of +RNA viruses [84,374], including lethal and economically important pathogens such as the severe acute respiratory syndrome coronavirus (SARS-CoV) and the arterivirus porcine reproductive and respiratory syndrome virus (PRRSV) [65,380]. Both viruses belong to the nidovirus order, which constitutes a group a viruses that is unique in that they employ a discontinuous RNA synthesis process to generate a set of subgenomic mRNAs that is used to express their 3′ encoded open reading frames (ORFs). Moreover, they encode a complex set of replicative proteins or non-structural proteins (nsps) to catalyse RNA synthesis [35,58]. Not all enzymatic functions are crucial for nidoviral RNA replication, but those that are, are all conserved in equine arteritis virus (EAV). Aided by its more compact genome, inability to infect humans and robust reverse genetics system, this prototypic arterivirus has become one of the best-studied nidovirus models [58,381].

Of the conserved enzymatic functions in nidoviruses, the RNA helicase domain is the most conserved. Like most helicases, this helicase is assumed to couple ATP hydrolysis to the translocation along one strand of a double helix in order to displace the other strand [108,110]. Biochemical evidence suggests that the nidovirus helicases have a strict 5′-to-3′ directionality during unwinding, but it is presently not known how their translocation is coupled to unwinding. Based on extensive theoretical, structural, biochemical and single-molecule studies, it is assumed that helicases generally use either a passive mechanism, in which case the transient fraying of the fork is trapped by the translocating helicase, or an active mechanism that relies on ATP hydrolysis to directly destabilise the hydrogen bonds at the fork [382,383,384,385,386,387,388]. As a consequence, a passive helicase is strongly controlled by the free energy of fork melting (ΔG°_{melt}, which depends on the sum of the free energy of hydrogen bond formation and the stacking energy [15,389]) and therefore the GC-content of the template. An active

helicase on the other hand will be relatively insensitive to the nucleic acid sequence that it has to unwind [382].

To gain insight into the unwinding dynamics of the nidovirus RNA helicase and the abilities of SF1 RNA helicases in general, we here show a magnetic tweezers (MT)-based single molecule assay that allowed us to follow the 5′-to-3′ strand displacement dynamics of EAV nsp10. Specifically, we used nsp10's ability to unwind RNA and DNA with equal efficiency and tethered a ~1 kb long DNA hairpin between a paramagnetic bead and glass-surface, and monitored the nsp10-driven change in the tether's end-to-end distance. We observed that nsp10 was able to couple hydrolysis of all four RNA nucleotides to the unwinding of this hairpin, but that the unwinding rate and pause frequency was strongly dependent on the nucleotide used. Furthermore, when we related the unwinding rate and pauses to the template sequence, we found that nsp10 was sensitive to the GC-content when hydrolysing ATP, GTP and UTP, but insensitive in the presence of CTP. These results suggest that this type of viral helicase is able to switch between a passive and active mode and that the coupling between NTP hydrolysis, translocation and active fork stabilisation is more flexible than was previously assumed.

Results and discussion

The EAV RNA polymerase nsp9 does not have strand-displacement activity

The EAV replication and transcription complex (RTC) is assumed to be anchored to cellular membranes, and to consist of a host factor and at least 13 viral non-structural proteins [313,380]. Similar to many other +RNA viruses, these enzymes include an RNA-dependent RNA polymerase (RdRp, nsp9) and the RNA helicase (nsp10) [390]. However, unlike various other well-studied viral RTCs, such as those of poliovirus or HCV, it is not known whether the RdRp has strand-displacement activity of its own, with the helicase playing merely a supporting role. To investigate this, we developed an EAV nsp9 assay in which we could test whether the processivity of this *de novo*-initiating RdRp [196] could be frustrated by placing a duplex region downstream of the initiation site in its template.

As was previously shown, EAV nsp9 prefers to initiate RNA synthesis on polyU repeats in the presence of [α-^{32}P]ATP [196,325]. However, when all nucleotides are present in the reaction, only low-molecular weight RNA products are formed on $polyU_{18}$ (Fig. S1A), suggesting that polymerisation is inherently limited on this template. To test whether processivity could be stimulated on heteromeric templates, we designed a template (denoted Hel11R) with a 3′ 10-nt long polyU initiation site and a downstream 20-nt long heteromeric region with relatively limited secondary structure. As shown in Fig. S1A and S1B, nsp9 was able to synthesise significantly longer products on Hel11R, using either [α-^{32}P]ATP or [α-^{32}P]CTP incorporation as readout. Interestingly, we also observed that none of the products was of template length (*i.e.*, a 30-mer) and the [α-^{32}P]CMP

incorporation signal only appeared in >4-mer products, suggesting that EAV nsp9 was initiating internally on the 3′ uridine repeat and specifically using the heteromeric region for extension.

To test the influence of dsRNA structures on the EAV nsp9 activity, we hybridised an oligonucleotide that was fully complementary to the heteromeric part of the template (denoted Hel1R). A 5′ polyU tail was added to this template to create a forked substrate and rule out that high molecular weight products were formed through primer-dependent extension of the hybridised oligonucleotide. Strikingly, all extension activity was lost in this duplex configuration, whereas initiation products were still present (Fig. S1B and S1C). Similar results were obtained with a non-tailed, but 5′ 3′dA-blocked complementary oligo. These results thus lead us to suggest that unlike many other viral RdRps, EAV nsp9 does not have strand displacement activity of its own and would thus have to fully rely on the helicase activity of nsp10 or other (cellular) enzymes with helicase activity during replication.

Biochemical characteristics of EAV nsp10

Previous studies of the EAV RNA helicase nsp10 were performed with maltose binding protein (MBP)-tagged nsp10 preparations and demonstrated that, like the coronavirus helicase nsp13 [109], EAV nsp10 was able to unwind both RNA and DNA with a 5′-to-3′ polarity in the presence of ATP [110]. However, these experiments focused only qualitative rather than quantitative kinetic results, which could have potentially masked differences in the unwinding efficiency. In addition, MBP is a relatively large tag (42 kDa) compared to the 51-kDa nsp10 and could have modulated the dynamics of EAV nsp10. We therefore readdressed the substrate specificity and biochemical characteristics of EAV nsp10 using purified N-terminally his_6-tagged EAV nsp10 (Fig. 1A).

Using single cycle assays (Fig. 1B), we tested nsp10's ability to displace a 5′ ^{32}P-labelled RNA or DNA oligonucleotide that was part of a dsRNA or dsDNA substrate in the presence of optimal 4 mM Mg^{2+} and near-saturating 2 mM ATP concentrations (Fig. S2). Aliquots were taken at various time points and analysed by native PAGE and autoradiography as exemplified in Fig. 1C. In line with previous observations, the unwinding efficiencies on DNA and RNA were essentially comparable and burst rates on DNA and RNA templates ($k_{DNA}$and k_{RNA}) obtained from single exponential fits to the single-cycle data revealed near-identical values: k_{DNA} = 0.015 ± 0.007 s^{-1} and k_{RNA} = 0.016 ± 0.004 s^{-1} (fitted value ± 95% confidence interval). We next explored the influence of the single-stranded 5′ loading region on the initiation of dsDNA unwinding by varying the length of the 5′ tail from 0 to 20 nt. In line with observations previously made for SARS-CoV nsp13 and other helicases [391,392], the unwinding rates decreased with a reduction of the tail length (Fig. 1E) and we found that nsp10 required at least a 10-nt single stranded loading platform to display significant unwinding activity.

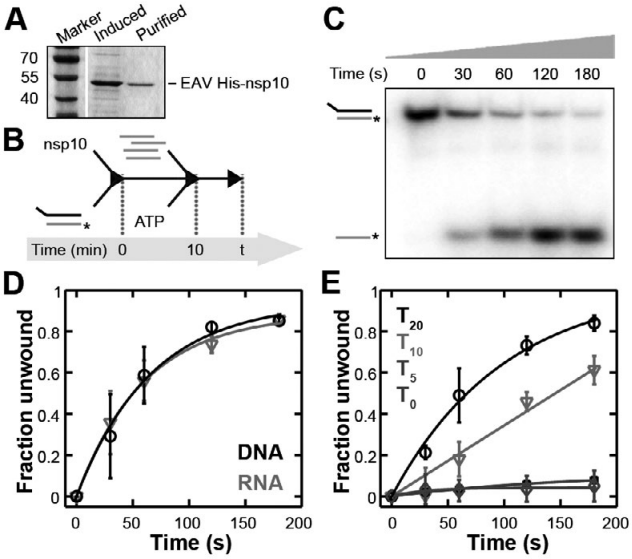

Figure 1: Template requirements of EAV nsp10. (**A**) SDS-PAGE analysis of purified N-terminally His_6-tagged EAV nsp10. The migration speed of his_6-nsp10 was in line with its expected molecular weight. (**B**) Schematic of the steps in the single-cycle assay. First, helicase (nsp10) and template consisting of a 5′ ^{32}P-labelled release strand (asterisk-labelled grey line) and an unlabelled loading strand (black line) were allowed to form a complex, before ATP and the unlabelled trap strand (grey lines) were added to the reaction. Next, samples were taken at time points t and these were resolved by native PAGE. (**C**) Example time course of nsp10 helicase activity in the presence of 2 mM ATP on dsRNA with a 20-mer overhang. Samples were resolved on 15% native PAGE and analysed by autoradiography. (**D**) Comparison of nsp10 unwinding activity on dsRNA (light grey triangles) and dsDNA (black circles) in the presence of 2 mM ATP. Both templates had a 20-mer overhang. The dsRNA curve was fit with using Eq. 1 with k_{RNA} = 0.015 ± 0.007 and A = 0.94 ± 0.06. For the dsDNA curve variables were k_{DNA} = 0.016 ± 0.004 and A = 0.88 ± 0.08. (**E**) To test the dependency of the EAV nsp10 unwinding activity on its ability to load, the 5′ single-stranded overhang of the loading strand was varied from a blunt-end (squares), a 5-nt T-tail (lozenges), a 10-nt T-tail (triangles), to a 20-nt T-tail (circles). K_{T20} was 0.009 ± 0.003 and A_{T20} 0.99. All experiments were performed in the presence of 2 mM ATP.

Design of magnetic tweezers construct and instrument calibration

To extend our study of EAV nsp10 in more detail and observe its unwinding dynamics in real-time, we employed our knowledge of its template specificity to design a MT experiment. Given the observation that EAV nsp10 unwinds dsDNA and dsRNA with similar efficiency, we opted to use a long DNA hairpin tether instead of a short RNA hairpin. Furthermore, to get insight in the behaviour of this enzyme on a natural sequence, we partly based this hairpin on the EAV genomic 3′ end.

Our MT setup consisted of a glass flow cell (Fig. 2A) in which the DNA hairpin was fixed between a paramagnetic bead and the glass surface through a pair of short DNA handles labelled with biotin and digoxigenin (Fig. 2B). On the 5′-side of the hairpin, a

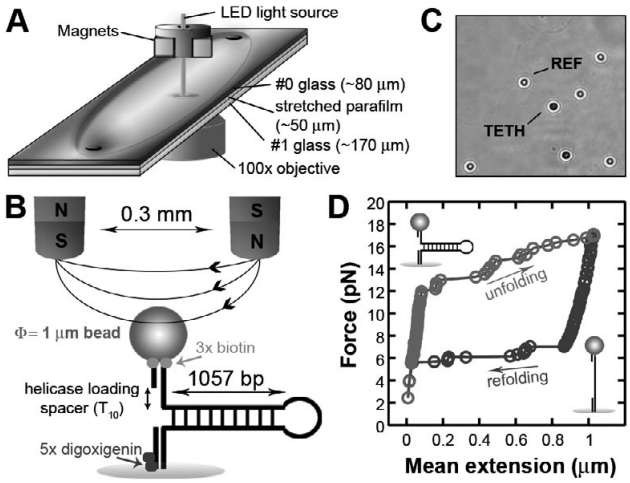

Figure 2: Magnetic tweezers setup. (**A**) Experimental setup of magnetic tweezers instrument. Two magnets are used to exert a force on paramagnetic beads that are tethered to the bottom surface of a thin flow cell consisting of stretched parafilm sandwiched between #0 glass (top) and #1 glass (bottom). Figure is not to scale. (**B**) The streptavidin-coated paramagnetic beads of 1 μm in diameter are tethered to the glass surface through a single DNA hairpin and multiple digoxigenin-anti-dig interactions. Permanent magnets are placed in a vertical alignment to achieve a sufficiently strong magnetic field to unwind the hairpin. For details about the hairpin construction, see Fig. S10. (**C**) Example microscopic field of view with reference beads (REF) and tethered beads (TETH). (**D**) Mechanical unfolding of the 1057-nt long DNA hairpin is achieved by bringing the magnets closer to the top surface of the top glass slide of the flow cell. The hairpin is fully unfolded at 16-17 pN.

short, T_{10} ssDNA region was created to provide a minimal platform for EAV nsp10 loading, thus minimising the chance of loading multiple active nsp10 molecules onto the template. Bound tethers were manipulated through a magnetic field created between two horizontally aligned permanent magnets and the bead (Fig. 2A and 2B).

As discussed elsewhere, the camera acquisition frequency (f_s, here 100 Hz) limits the calibration of the applied force [393], while the Brownian motion of the tethered bead and the intrinsic resolution of the MT instrument essentially limit the resolution at which the tether length can be measured to ~1 nm [394]. However, this limit can only be achieved through the use of smaller beads and shorter nucleic acid tethers, which in turn constrain the force range that can be applied to the tether and the confidence with which the magnetic field can be calibrated [393]. In an attempt to optimise all conditions for our experiments, we employed monodisperse 1 μm beads so we could use a calibration of the magnetic field to estimate the applied force within 10% error [393]. In addition, we used a DNA hairpin with relatively short handles to minimise the initial tether length, and a stronger magnetic by reducing the magnet gap-size to 0.3 mm and decreasing the non-accessible range of our flow cell (*i.e.*, the distance between

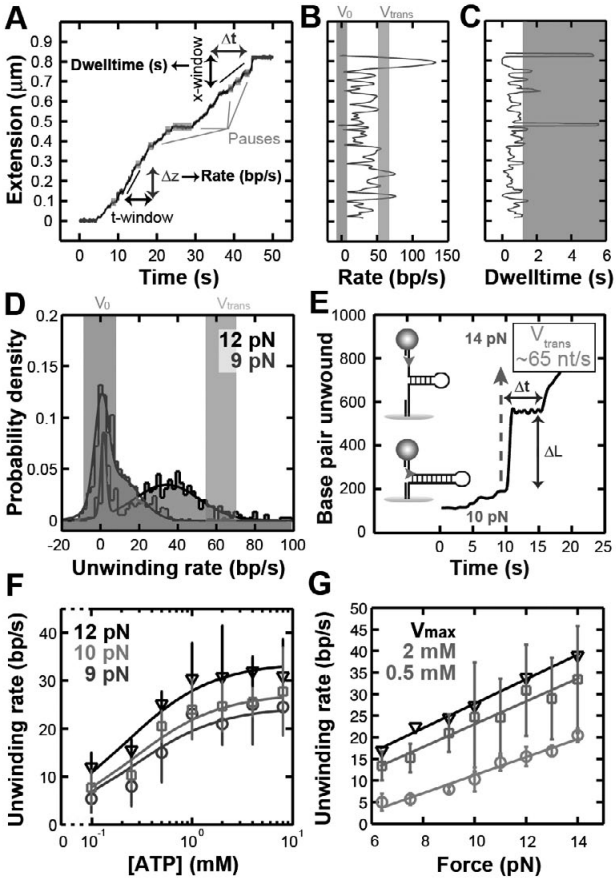

Figure 3. dsDNA unwinding by EAV nsp10 in the presence of ATP. (**A**) Analysis of the extension traces is performed by a dwell time analysis using a fixed 10-bp sliding window in z and a rate analysis by applying a fixed 0.9-s (90 points) sliding window in t. Pauses identified using either of these methods are indicated in dark grey. Experiment was performed at 10 pN force and 2 mM ATP. (**B**) Velocity and (**C**) dwell time analysis of the nsp10 activity along the activity trace. Pauses are indicated in dark grey and the translocation velocity (V_{trans}) in light grey. (**D**) Analysis of the instantaneous unwinding rates of EAV nsp10 at 2 mM ATP shows a pronounced peak around 0 ± 3.4 bp/s (mean ± sd) for 9 pN (indicated in dark grey) in addition to the unwinding peak centred around 21 bp/s at 9 pN. The unwinding peak at 12 pN is centred around 31 bp/s. The light grey bar indicates V_{trans}. (**E**) To measure the translocation rate of EAV nsp10, the helicase was first allowed to initiate at a constant force of 10 pN. Then the dsDNA template was quickly converted into a partial ssDNA template by increasing the applied force to 14 pN. At this force, the hairpin forms a stably folded intermediate. The distance covered by the helicase (ΔL) and the time required to do so (Δt) provide us with a measure of V_{trans}, which we estimated at 65±13 nt/s. (**F**) Mean unwinding rates as function of the ATP concentration for EAV nsp10 at 9 (circles), 10 (squares), and 12 pN force (triangles). At all forces investigated, the unwinding rate obeys Michaelis-Menten kinetics with K_m = 0.24-0.26 mM. (**G**) Unwinding rates at 0.5 (circles) and 2 mM ATP (squares) and maximum unwinding velocities (V_{max}, triangles) obtained from Michaelis-Menten kinetics plotted as function of the applied magnetic force.

the top of the tethered bead and bottom of the magnets, a value that would be zero if we they could physically touch) to 130 µm (Fig. 2A and 2B). As shown in Fig. S3 and S4, these modifications allowed us to apply forces up to 20 ± 2 pN and track reference beads through microscope-based image analysis (Fig. 2C) with a vertical standard deviation of ~1.4 nm and tethered molecules with a resolution of ~3.0 nm in z (Fig. S4).

Single-molecule assay and ATP dependency

Unwinding or mechanical unfolding of the hairpin results in an increase in the distance between the flow cell surface and the magnetic bead. Additionally, a force that is applied perpendicular to the fork junction lowers the free energy that the helicase has to overcome to unwind the duplex with ΔG_f. Consequently, at forces where $\Delta G_f > \Delta G^\circ_{melt}$, the hairpin will spontaneously unfold. To identify the force at which our 1057-bp hairpin was stable, we first mechanically unfolded the hairpin in absence of helicase (Fig. 2D). Analysis of the mechanical unfolding demonstrated that the hairpin remained stably folded up to forces of 12 ± 1 pN (Fig. 2D). In addition, we observed that over 16 ± 2 pN was required to fully unwind the DNA duplex and that refolding of the hairpin occurred at 6.4 ± 1 pN (Fig. 2D).

When we next added ATP and EAV nsp10 to the flow cell, we observed changes in bead height. The most common event at 9-14 pN and 2 mM ATP was a steady increase in extension up to the entire single-stranded length of the tether (Fig. 3A). No rezipping or refolding was observed when the helicase reached this position. Typically, the instantaneous unwinding rate - computed from the slope of a running window along the time axis (Fig. 3A and 3B) - and the dwell time of the helicase fluctuated along the template, and we occasionally observed interruptions or pauses in the extension (Fig. 3). The latter we defined as those positions in the template where the unwinding rate was within 0 ± 7 bp/s (mean ± 2 standard deviations; Fig. 3D, orange area). At lower forces and reduced ATP concentrations, we also observed a rapid refolding of the hairpin (Fig. S5), likely because the helicase was more prone to dissociation under these conditions. To ensure that we were measuring the kinetics of a single nsp10 helicase, we tested dilutions of the helicase preparations and found consistent behaviour up to the lowest concentration tested, *i.e.*, 2 nM of helicase monomer (Fig. S5E and S5F).

To investigate whether the nsp10 helicase unwinding rate would ultimately approach the translocation rate (V_{trans}), we performed an experiment in which the helicase was first allowed to initiate unwinding at a constant force of ~10 pN. Once helicase activity was detected, we rapidly increased the applied force to ~14 pN (Fig. 3E), which resulted in a stably folded intermediate that had opened by ~550 bp relative to the fork junction of the fully folded hairpin (Fig. 2D). We next recorded the time Δt that the helicase required to travel along the created single stranded template with length ΔL and initiate a second unwinding event at the new fork (Fig. 3E). The helicase translocation rate was

obtained from ΔL / Δt and found to be ~65 ± 13 nt/s. When we now apply this value to local unwinding rate observed in Fig. 3B, we find that occasionally, the helicase did indeed approach this rate. In addition, we also observe extension locations where the unwinding rate appeared to have exceeded the translocation rate. Closer inspection shows however, that these fast events coincide with abrupt changes in the extension, which suggest that they are derived from short spontaneous unfolding events of the hairpin whose rates (typically ~1000 bp/s [395]) got averaged to lower rates by our 0.9 s sliding window.

The direct measurement of the helicase activity on the double-stranded template gives insight into the coordination between ATP hydrolysis and unwinding. Specifically, by varying the ATP concentration ([ATP]) we were able to obtain the Michaelis-Menten constant, K_m of ATP. This value was ~0.26 mM and independent on the applied force (Fig. 3F). Furthermore and consistent with the reduction of the energy barrier for duplex unwinding, an increase in the applied force gave a strong linear increase in the unwinding rate over the force range that could be measured (Fig. 3G). This increase was consistent among various ATP concentrations and the V_{max} obtained for the Michaelis-Menten fits. Interestingly, previous single-molecule studies observed fundamentally different behaviours for the relation between the unwinding rate and the applied force, including no force-dependence at all for the SF2 helicase NS3 of HCV [376] and a non-linear dependence for the hexameric helicases of T7 and T4 [383,395]. Comparable dependencies were found in our dwell time analysis, which used a sliding window of 10 nt over the extension axis (Fig. S6).

EAV nsp10 is a promiscuous helicase

It is known that some helicases are not strictly specific for ATP hydrolysis when they unwind a nucleic acid template [373]. For instance, the hexameric T7 helicase can utilise all dNTPs and NTPs except CTP and GTP in both bulk and single-molecule experiments [396,397]. Interestingly, we found in our bulk experiments that EAV nsp10 was highly promiscuous as well, and able to utilise ATP, dATP and CTP with similar efficiency for unwinding activity (Fig. 4A and 4B). Lower efficiencies were observed when we performed the reaction in the presence of UTP, GTP or ribavirin triphosphate, a ATP and GTP analogue commonly used to treat viral infections [56].

We next focussed on nsp10's ability to use the ribonucleotides in our single-molecule assay. When experiments were conducted in the presence of 2 mM CTP, we essentially found similar mean unwinding velocities as in the presence of 2 mM ATP (Fig. 4C). In line with our bulk experiments, lower unwinding velocities were observed in the presence of UTP and GTP (Fig. 4D). However, processive unwinding was strikingly more often interrupted with pauses (Fig. 4E) and refolding events in the presence of ATP, UTP and GTP compared to CTP. Although we believe that the latter may be attributed to the helicase

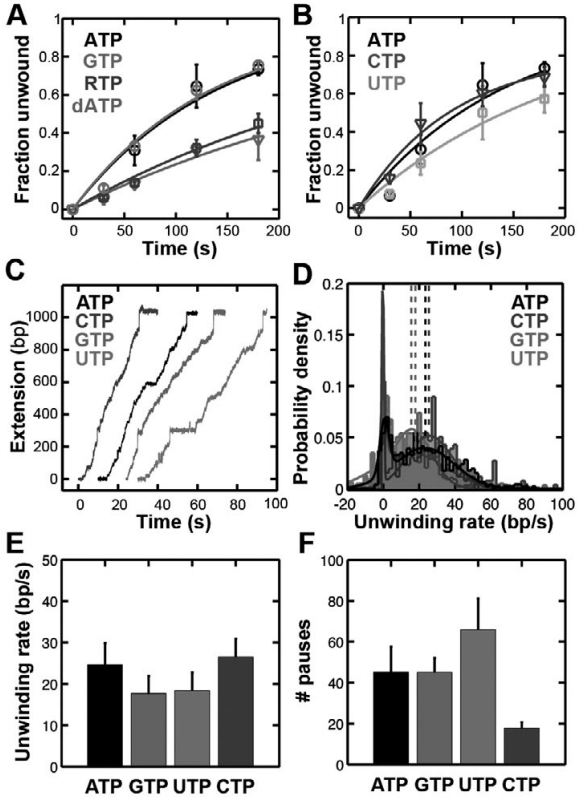

Figure 4. Use of different NTPs modulates the nsp10 dsDNA unwinding rate. (**A**) Bulk assays were performed to test nsp10's ability to use different nucleotides for dsRNA unwinding. Clearly, both ATP and dATP could be used with similar efficiency, suggesting that the enzyme does not discriminate between the sugar moiety on the NTPs. Differences were observed for the other purines GTP and RTP at an equal concentration of 2 mM. (**B**) Nsp10 was also able to efficiently unwind dsRNA in the presence of 2 mM CTP, but showed slightly lower kinetics in the presence of 2 mM UTP. All 4 traces were taken at 10 pN. (**C**) Single-molecule unwinding traces of EAV nsp10 in the presence of 2 mM of CTP (dark grey), ATP (black), GTP (light grey) and UTP (ultralightgrey). Experiments were performed at 10 pN assisting force. (**D**) Probability densities of the unwinding velocities of the EAV nsp10 in the presence of 2 mM ATP, CTP, GTP or UTP. and UTP. Experiments were performed at 10 pN. Dashed lines indicate the centres of the Gaussian fits. (**E**) On average, we found that CTP and ATP gave similar mean instantaneous unwinding rates at 10 pN, whereas unwinding in the presence of GTP and UTP was lower on average, but not significantly. Error bars represent standard deviations. (**F**) Analysis of the average number of pauses per unwinding event at 10 pN demonstrated significant differences between unwinding in the presence of CTP and the other three nucleotides.

dissociating from the template, the former may also be related to sequence-dependent pausing and the unwinding mechanism that the helicase uses to separate the strands (see below).

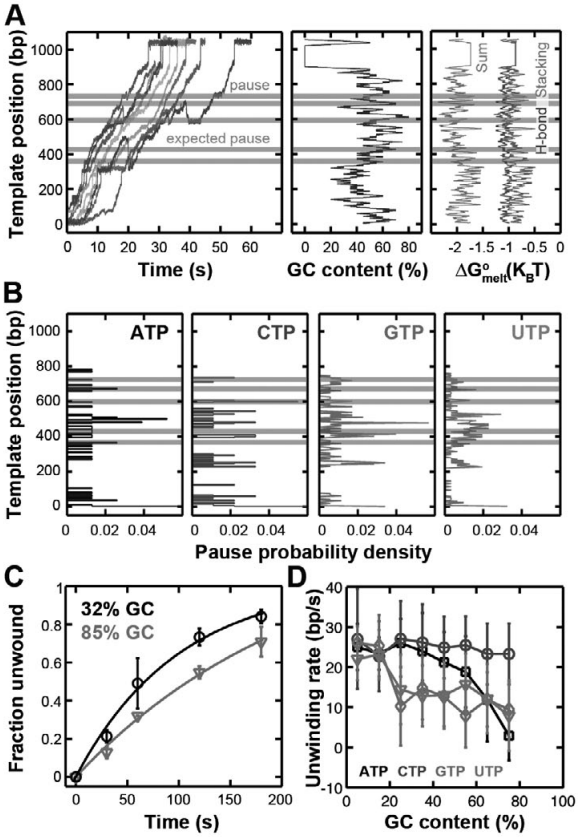

Figure 5. EAV nsp10 can switch between passive and active nucleic acid unwinding. (**A**) Example of aligned traces taken for unwinding at 10 pN and 2 mM CTP (left panel). Identified pauses that corresponded to a high GC content in the template (middle panel) and a correspondingly low ΔG°_{melt} are indicated in grey (right panel). The GC content and ΔG°_{melt} were calculated for a running window of 10 bp. ΔG°_{melt} was calculated as the sum of the hydrogen bonding energy (dark grey) and stacking energy (light grey) [15,389]. (**B**) At certain positions, no pauses were observed in CTP traces (2nd panel), but clearly evident in helicase unwinding events obtained in the presence of ATP (1st panel), GTP (3rd panel) and UTP (4th panel). We have marked several of these different events with bars in panels A and B. (**C**) Unwinding efficiency of nsp10 on dsRNA templates containing a low (black circles) or high GC (grey triangles) content. Both experiments were performed in the presence 2 mM ATP. (**D**) Unwinding velocities were associated with their template position and corresponding GC-content over a 10-bp window. Unwinding rates were subsequently binned by their GC-content and fitted with the sum of three Gaussians to extract the mean unwinding rate and standard deviation (see Fig. S8). All experiments were performed under 10 pN assisting force.

Active and passive unwinding mechanisms

The above results of the fluctuating local unwinding rate and the difference between the translocation velocity on single-stranded nucleic acid should allow us to define whether nsp10 was using a passive or active unwinding mechanism in the presence of ATP. Such an estimate is important for the interpretation of the helicase function, because passive

helicases are typically involved in replication and allow for a tighter coupling between the helicase and the replicative polymerase than active helicases [383,388,395,398,399]. In eukaryotic cells, this strategy may facilitate co-ordination between leading and lagging strand synthesis, while active mechanisms appear to be mostly used for processes that are not strictly dependent on this co-ordination, such as DNA repair [382,400].

Previous single-molecule studies of helicases have attempted to define the helicase unwinding mechanism by fitting the observed unwinding velocity as a function of $\Delta G°_{melt}$, the helicase forward and backward translocation rates k^+ and k^-, the ΔG_f, the helicase step size n per ATP hydrolysis event, and an helicase-fork interaction potential ΔG_{int} in order to describe the helicase's ability to actively destabilise the fork [386]. Crucially, however, the fitting approach may lead to fundamentally different interpretations of ΔG_{int} depending on the assumed step size and the backward translocation rate [382], and did indeed result in different outcomes for relatively similar enzymes [383,395].

A more robust method is to interpret the helicase unwinding rate as a function of the sequence of the template, *i.e.*, the ratio between the velocity at high GC-content (V_{GC}) and 0 GC-content (V_{AT}) [382]. Specifically, if we follow Manosas *et al*. and set the threshold that separates an active from a passive mechanism at $\Delta G_{int} = 1\ K_BT$ or about half the averaged $\Delta G°_{melt}$ (Fig. 5A), we can predict that an active helicase advancing with 1-bp steps and a negligible backward translocation rate will loose at most 75% of its unwinding rate when going from a AT-rich to a GC-rich sequence [382]. Consequently, V_{GC} / V_{AT} will therefore exceed 25% for active helicases, while passive helicases should have a sequence-dependent unwinding ratio that is much smaller than 25%.

The unwinding mechanism of EAV nsp10 depends on the nucleoside triphosphate used for hydrolysis

To investigate the sequence dependence of EAV nsp10, we first aligned the helicase traces to improve the accuracy in relating the unwinding rate to the local GC content. Typically, we found that we could align the traces by their end point with 1 nm standard deviation (Fig. S8). We next used the pause probability density as function of the template position to get an estimate of the average drift and the accuracy of the alignment along the rest of the template. As shown in Fig. 4B and S8, we were able to identify pauses at GC-rich positions in the middle of the template with a standard deviation of 8 nm, suggesting that the error in sequence identification was ~5 nm per 250 nm (approximately 6 bp per 300 bp). This was comparable to the standard deviation of a tethered bead position in absence of helicase over the course of the longest experiments (Fig. S8).

Strikingly, the side-by-side comparison of the pause probability densities of the helicase in the presence of the four NTPs shows that they are not equal Fig. 4B). In general, we observe that the helicase has a probability to pause upstream of GC-rich sequences. However, this behaviour is only consistent for helicase unwinding in the presence of

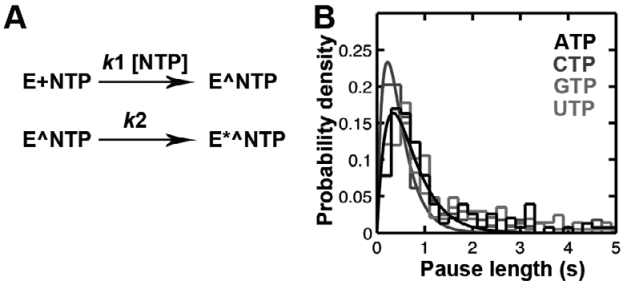

Figure 6: Pausing by nsp10 depends on two steps and nsp10 can switch between passive and active unwinding. (**A**) Similar to HCV NS3 [376], pauses that occur during template unwinding by EAV nsp10 can be fit with two irreversible kinetics events, one of which may present a NTP-dependent binding step, while the other may present a NTP-independent structural change in the enzyme, *e.g.*, in one of the two RNA binding domain. The first is a pseudo first order reaction involving nucleotide binding (k_1 [NTP]), while the second is NTP independent (k_2). (**B**) Pause duration histograms of nsp10 pause steps (0.2 s bins) in the presence of 2 mM ATP, CTP, GTP or UTP can be fitted with the an equation describing the sum of the two kinetic schemes of Fig. 6A as described previously [376]. Overall, the histograms of ATP, GTP and UTP can be well fit with k_1 = 1.5-1.7 10^3 M^{-1} s^{-1} and k_2 = 0.6-0.7 s^{-1}. The CTP histogram is best fit with k_1 = 2.9-3.0 10^3 M^{-1} s^{-1} and k_2 = 0.6-0.7 s^{-1}, suggesting that the nucleotide-dependent step is discriminating between the nucleotides.

ATP, UTP and GTP, and not in the presence of CTP (Fig. 4B). Also in our bulk experiments do we observe that helicase unwinding is more efficient on templates with a lower GC-content (Fig. 4C). When we next plot the unwinding rate of the helicase as function of the GC-content, we find that although the helicase loses 90% of its velocity when hydrolysing ATP, UTP or GTP on a GC-rich sequence, it is relatively insensitive to the template sequence when using CTP (Fig. 4D, Fig. S8). Consequently, when we apply the 25% threshold proposed by Manosas *et al*., we find that the helicase is effectively unwinding the template in an active mode in the presence of CTP, while it appears to unwind the template with a passive mechanism in the presence of the other nucleotides.

This observation appears to be supported by the analysis of the helicase pause durations in the presence of the different nucleotides (Fig. 6). Interestingly, we found that not only the unwinding velocity, but also the pause frequency during unwinding events is dependent on the ATP concentration (Fig. S9). This suggests that similar to HCV NS3, the exit from an EAV nsp10 pause is also nucleotide dependent. The shapes of the pause duration histograms are, however, not single exponentials and can be fit if we assume a kinetic mechanism that involves two steps of which only the first is nucleotide dependent (Fig. 6A). If we fit our data with such a two-step model, we find that that all nucleotides have the same nucleotide-independent rate, but that although the ATP-, GTP- and UTP-dependent pauses have the same rate for nucleotide binding, the nucleotide-dependent rate CTP rate is ~2 fold higher (Fig. 6B).

Concluding remarks

The work presented here provides a study of the nucleotide hydrolysis and nucleotide specificity of the SF1 helicase of EAV nsp10 and the coupling of these events to the mechanism that this helicase uses for nucleic acid unwinding. Our study indicate that in the presence of ATP, the most abundant nucleotide in the cell at 1-5 mM [401], nsp10 is dependent on the applied force and using a passive unwinding mechanism to displace the two template strands. In the presence of CTP on the other hand, whose intracellular concentration is ~0.2 mM, nsp10 appeared to unwind the double stranded template using an active mechanism [402].

Given the significantly higher intracellular ATP at homeostasis it appears likely that the default unwinding mechanism of EAV nsp10 is passive. Nevertheless, analysis of the unwinding mechanism of various helicases has so far always assumed that the coupling between hydrolysis, translocation and unwinding is fixed and either passive or active [382,383,386]. Here we demonstrate that this need not be the case and that their pairing may switch depending on the bound nucleotide. Interestingly, it was recently shown that the hexameric T7 helicase processively unwinds dsDNA in the presence of dTTP, whereas ATP-based unwinding induces backsliding as a result of the additional 2′-OH group on the ribose sugar [397]. Structural analysis revealed that this 2′-OH may displace the side-chain of nucleotide-binding residue Y535 and thereby alter the structural dynamics of the helicase and thus its affinity for the template [397]. Such changes are certainly not without precedent, as structural dynamics analyses of RNA polymerases have shown that local perturbations in the structure may induce significant changes in the overall behaviour of the enzyme and, in polymerases, the fidelity of nucleotide incorporation [177].

Structural data is presently unavailable for the nidovirus helicases, which makes it impossible to verify whether amino acid side-chains in the nucleotide-binding pocket could be repositioned upon CTP binding or whether this may affect the structural dynamics of the enzyme. We speculate, however, that such effects could well explain the switch that we observe here and hypothesise that a similar nucleotide-dependent coupling may be present in the active site of other helicases. Further, if local perturbations can influence the unwinding mode of the helicase, this would open up the existence of (co)factors that induce allosteric changes that favour one unwinding mechanism over the other and are thus able to regulate or frustrate the helicase's co-operation with enzymes in, *e.g.*, the replisome or the viral RTC.

Material and methods

Cloning, expression and purification of EAV nsp10

The coding region for EAV nsp10 in the Bucyrus genome (Genbank accession number NC_002532) was amplified by PCR from the EAV cDNA clone [403] using primers E779 and E789 (see Table S1). The PCR product was ligated into the Gateway cloning vector pDONR (Invitrogen) and subsequently subcloned into the T7 driven expression vector pDEST14 (Invitrogen) according to the manufacturer's protocol, thereby creating pDEST14-EAV-His-nsp10.

For expression, BL21(DE3) cells were transformed with pDEST14-EAV-His-nsp10 and grown on Luria Broth (LB) agar plates containing ampicillin (50 µg/ml). Next, 2000 ml LB-5052 [292]containing ampicillin (50 µg/ml) was inoculated with 50% of the colonies on the agar plate and grown to OD_{600}>1.0 at 37°C. Subsequently, the cells harvested and resuspended in 2000 ml LB containing amplicillin (50 µg/ml) and IPTG (1 mM) and grown at 37°C for a further 3-4 h. Cells were finally harvested by centrifugation and stored at 20°C until protein purification was started.

For purification, bacterial pellets were thawed on ice, resuspended in buffer A (20 mM This pH 8.5, 20 mM imidazole, 0.05% Tween-20, 5% glycerol, 5 mM β-mercaptoethanol and EDTA-free protease inhibitor cocktail (Roche)) containing 500 mM NaCl, and lysed by sonication. The supernatant was cleared by ultracentrifugation at 20,000 *g* for 30 min and subsequently incubated with Talon beads (Clontech) for 2 h at 4°C. The beads were washed four times 15 min with 20 volumes of binding buffer. Ultimately, the N-terminally His_6-tagged helicase was eluted with 150 mM imidazole in buffer A containing 500 mM NaCl and immediately gelfiltrated with a supradex 200 column (GE Healthcare) in buffer A containing 300 mM NaCl. Nsp10 containing fractions were subsequently pooled, dialysed, stored and analysed as described previously for SARS-CoV nsp12 [154].

Polymerase and unwinding assays

EAV nsp9 was purified and analysed as described previously [325]. For EAV nsp10 unwinding assays, a total of 100 nM of purified EAV nsp10 was incubated with 1 nM 5′ ^{32}P-labelled RNA or DNA duplex substrate at 22 °C for 10 minutes in reaction buffer (Tris-HCl pH 7.5, 20 mM NaCl, 0.01 mg/ml BSA, 5% glycerol, 0.01% Triton X100). Prior to the addition of 2 $MgCl_2$ and 2 ATP, unless stated otherwise, the reactions were cooled down to 15 °C and 1 µM unlabelled release strand added to trap unbound helicase (Fig. 1B). Samples were taken at the indicated time points and quenched with an equal volume of quenching buffer (20 mM Tris-HCl pH 8.0, 50 mM EDTA, 60% glycerol, 0.5% SDS and 0.1% bromophenol blue)

After gel electrophoresis on 15% native PAGE gels, the fraction unwound was analysed via autoradiography. Next, the fraction of unwound nucleic acid was plotted against the

reaction time and fitted to a single-exponential equation as described previously uning Eq. 1 [391,404]:

$$F(t) = A(1 - ep(-kt)) + C \quad \text{[Eq. 1]}$$

Here, *F(t)* is the fraction of template unwound at time *t* in seconds, *A* the amount of unwound product, C the correction for the amount of unwound product present in the beginning of the reaction, and *k* the pseudo first order rate constant of nucleic acid unwinding.

DNA hairpin construction

The hairpin representing the 3′ 990 nt of the EAV genome was amplified by PCR from the EAV cDNA clone [403] using primers 513 and 514. This product was digested with KpnI and XhoI, and hybridised to hairpin oligos 515-518 (see table S1 and Fig. S10) in annealing buffer (10mM Tris pH 7.9, 50 mM NaCl, 1 mM DTT, and 10 mM $MgCl_2$). After ligation with T4 DNA ligase (New England Biolabs) in annealing buffer with 1 mM ATP, the products were gel purified and labelled with digoxigenin-UMP at their 3′ end using Klenow polymerase. Final products were cleaned using YM100 columns (Millipore) and stored at -20 °C in TE (20 mM Tris-HCl pH 8.0, 10 mM EDTA).

Magnetic tweezers and flow cell configuration

We used a custom built MT setup similar to that developed and described by Strick *et al*. [337], albeit it with technical modifications. Briefly, a CCD camera with a acquisition frequency of 100 Hz (Dalsa) was used to track monodisperse superparamagnetic beads of 1.0 ± 0.1 µm in diameter (MyOne beads, Life Sciences) tethered to the surface via the hairpin construct (~1.0 µm fully unzipped, see Fig. 2D). Focusing of the 100x oil-immersion objective (Olympus) was achieved with a pifoc (P-726.1CD, Physik Instrumente) that was fixed onto a 25-mm thick aluminium base plate and encased in a stage (Merzhauser).

As magnets, we used two gold-plated (Ni-Cu-Ni-Au), 5 x 5 x 5 mm neodymium-iron-boron (NdFeB) permanent magnets (SuperMagnete, Germany) that were placed 0.3 mm apart in an aluminium holder. Flow cells were constructed using a #1 nitrocellulose-covered microscope coverslip as bottom slide and a #0 coverslip as top slide (VWR International). As spacer between the two slides we used manually stretched parafilm, which we found to have an average thickness of 50 ± 5 µm. Overall, this layout resulted in a flow cell thickness of ~300 µm and a minimal magnet-to-surface distance of ~130 µm (Fig. 2B).

Magnetic tweezers calibration

To be able to correct for mechanical drift during the MT experiments, 1.0 µm polystyrene beads (Polysciences) were baked onto the surface by first adsorbing them to the bottom slide of the flow cell in 10 mM Tris pH 8.0 and 100 mM $MgCl_2$ and next fixing them through baking at 100 °C for 3 min. During measurements, mechanical drift was minimised by correcting the tethered bead height relative to the 1-µm reference bead every 20 frames. Before use, the inner surfaces of the flow cell were passivated with bovine serum albumin (BSA, 10 mg/mL). The extension-to-nucleotide conversion was calibrated as described previously (Fig. S3D) [383,395]. The reference bead fluctuations could be tracked with a standard deviation of ~1.4 nm in z, and ~0.6 nm in x- and y-directions (Fig. S4). Tethered MyOne beads could be tracked with a standard deviation of ~3 nm within the force range of our experiments (Fig. S4). To calibrate the decay of the magnetic field and the applied magnetic force, a 20.7 kbp dsDNA (~7.0 µm) tethered to MyOne beads was used (Fig. S3). Spectral corrections were performed as described previously [393].

Single-molecule helicase experiments

Hairpin DNA tethers were prepared by binding 1 ng of hairpin DNA to 2 µl MyOne beads in 10 µl binding buffer (20 mM Tris-HCl pH 7.5, 5 mM EDTA, 100 mM NaCl, 0.01 mg/ml BSA and 0.01% Tween-20) at 20 °C for 15 min. Tether-bead complexes were taken up in a final volume of 100 µl and introduced into the flow cell at 10 ml/min and incubated for 60 min in absence of the magnetic field. Flow cells were next washed with 0.5 ml helicase buffer (20 mM Tris-HCl pH 7.5, 20 mM NaCl, 4 mM $MgCl_2$, 0.01% Triton X-100 and 0.01 mg/ml BSA) before the introduction of 2mM ATP and 20 nM helicase in helicase buffer, unless noted otherwise for specific experiments.

Data analysis

Helicase unwinding events were identified by thresholding the end-to-end change in z to 2 standard deviations beyond the mean z-position at the beginning of each measurement. To estimate instantaneous helicase unwinding velocities from the end-to-end measurements, traces were first median filtered at 1 Hz and aligned by the their fully unwound extension where possible. Slopes were then fitted to the data points in fixed 90-point windows, which were moved by 10 points along the time axis. Pauses and non-zero velocities were identified by fitting unwinding rate histograms of 2-bp/s-bins with the sum of three Gaussians (one for negative rates, one for pauses, and one for positive rates). Pause positions were subsequently extracted by thresholding the velocities at consecutive time axis windows to 2 standard deviations of the zero velocity peak. Dwell times were extracted from the traces by moving a 10-bp window along the extension axis with standard deviation intervals of the fluctuations in the z-position.

Acknowledgements

The authors thank Dr. Jan Lipfert, and Dr. Iwijn de Vlaminck for stimulating discussions and assistance with programming, Dr. Jacob Kerssemakers for discussions and his assistance with the development of the flow cell, and Dr. Michelle Spiering and Dr. Stephen Benkovic for sending hairpin DNA for testing. This work was supported by the Netherlands Organization for Scientific Research (NWO) through Toptalent grant 021.001.037 to AV and TOP-GO grant 700.10.352 to ES and ND.

CHAPTER 7 - SUPPLEMENTAL INFORMATION

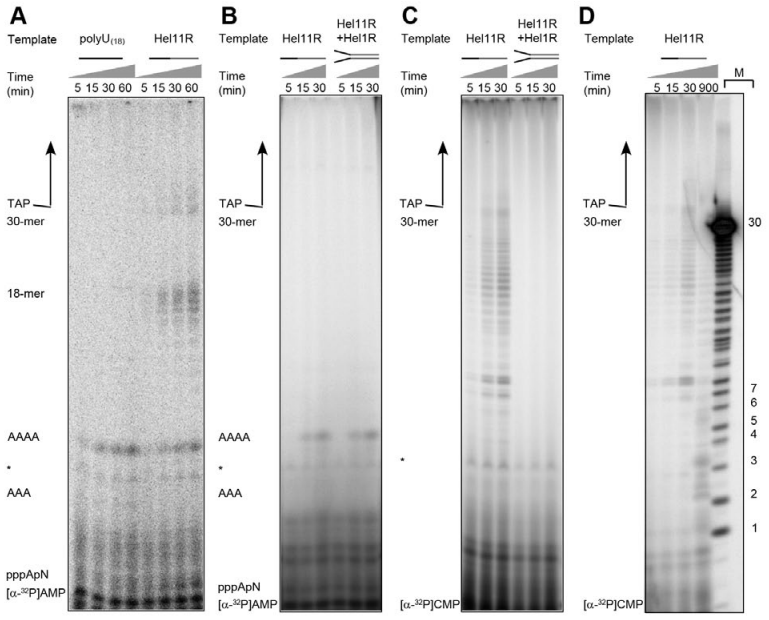

Figure S1. Activity of EAV nsp9 is influenced by dsRNA. (**A**) Purified EAV nsp9 [325] can synthesise oligomeric RNA products in the presence of uridine repeats (black line in template schematic) in the polyU$_{18}$ or the Hel11R template, and 0.17 μM [α-^{32}P]ATP, 50 μM ATP and 100 μM CTP, GTP and UTP. (**B**) Similar oligomeric products are formed in the presence of only [α-^{32}P]ATP, 50 μM ATP and Hel11R (left panel), or [α-^{32}P]ATP, 50 μM ATP and the partially duplex template consisting of oligos Hel11R and Hel1R (right panel). (**C**) When [α-^{32}P]ATP is replaced with [α-^{32}P] CTP RNA products >5-mers are observed only when nsp9 is incubated with the single stranded Hel11R, but not with the oligo duplex. Together with the results of Fig. S1B, these observations suggest that the duplex specifically inhibits extension. (**D**) nsp9 polymerase activity on the Hel11R template relative to the NaOH degradation of a 5′ ^{32}p-labelled Hel11R to indicate the expected RNA product length if nsp9 was initiating RNA synthesis on the terminal 3′ U of the templates. We note that the size distribution of the smaller 5′ ^{32}P-labelled products should not be compared to the migration pattern of synthesised RNA products (which contain 5′ triphosphates) due to their different negative charge and migration velocity in the electric field of the 20% 7M Urea gel.

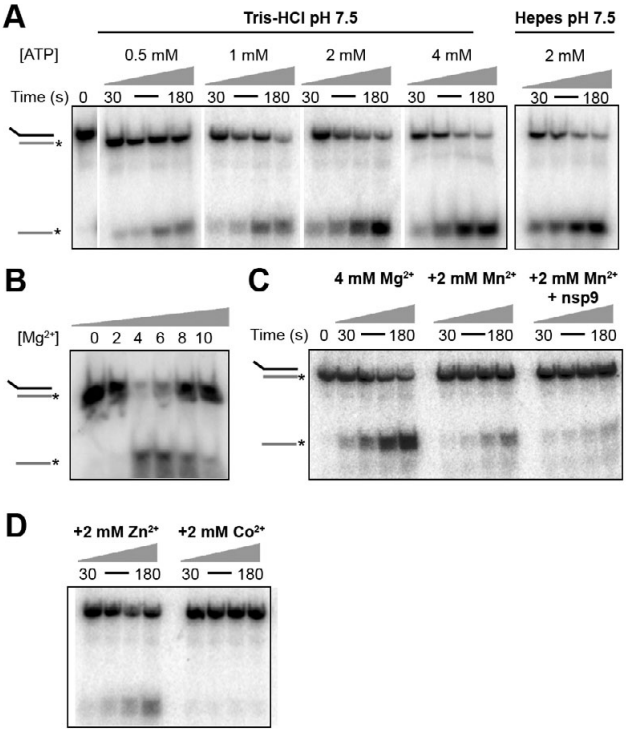

Figure S2. Biochemical characteristics of EAV nsp10. (**A**) Purified nsp10 was incubated with 5′ tailed RNA duplexes and assessed for its ability to displace the 5′ ^{32}P-labelled bottom strand (grey and labelled with asterisk) in the presence of various concentrations of ATP, 4 mM $MgCl_2$ and either a 20mM Tris-HCl or 20 mMHepes buffer. (**B**) The ability of nsp10 to unwind dsRNA in the presence of various concentrations of Mg^{2+}, 2 mM ATP and 20mM Tris-HCl. (**C**) When Mn^{2+} - required for *de novo* RNA synthesis of EAV nsp9 *in vitro* - was added to helicase reactions containing 2 mM ATP, the ability of nsp10 to unwind the provided dsRNA template was significantly reduced both in the presence and absence of nsp9 polymerase. (**D**) Similar to the effect of Mn^{2+}, the addition of Zn^{2+} or Co^{2+} could interfere with nsp10's unwinding efficiency in the presence of 2 mM ATP.

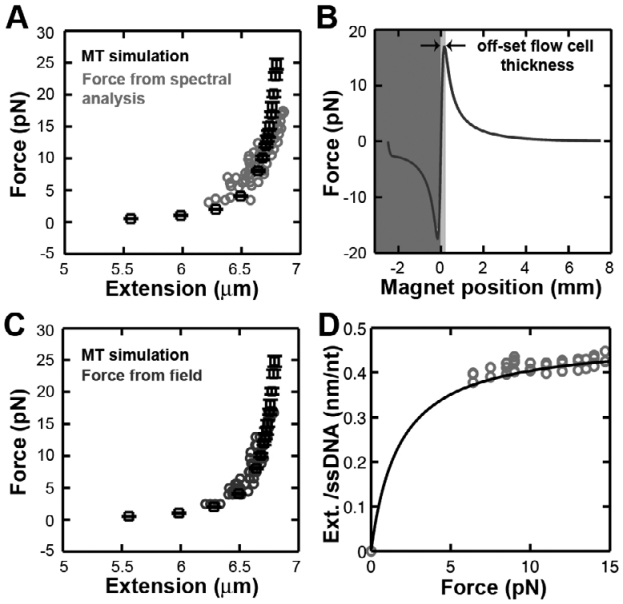

Figure S3. Force calibration and nm to bp conversion. (**A**) It is generally feasible to measure the force exerted by the magnetic field on the DNA molecule by recording the fluctuations of the bead's position and analysing these positions used previously discussed spectral analysis procedures [393]. However, given the short contour length of our 1057-kb hairpin in both the folded and unfolded configuration, the high cut-off frequency associated with this tethered-bead system, and the limited acquisition frequency of our camera (100 Hz) we were not able to perform a reliable direct measurement (*i.e.*, with an error <10%) of the applied magnetic force on these tethered beads. We therefore calibrated the magnetic field and used the low polydispersity (<10%) of the MyOne beads to estimate the applied magnetic force. To calibrate the magnetic field in our flow cell, we tethered 20.7-kb (~7 μm) dsDNA molecules to MyOne beads and measured their extension as function of the magnet position. The applied magnetic force was then computed using spectral analysis and plotted against the extension for three tethers (light grey circles). For reference, a simulated force-extension curve (including spectral analysis of the simulated data) of a ~7 μm dsDNA tether is shown (black squares). Error bars depict standard deviation of 5 simulations. (**B**) Magnetic field gradient computed for various magnet positions as described previously [405], using vertical 5x5 mm magnets that were placed 0.3 mm apart and 1 μm MyOne paramagnetic beads. The flow cell thickness is indicated in light grey (**C**) dsDNA molecules of 21-kb (~7 μm) were tethered to MyOne beads and we measured their extension as function of the magnet position. Using the field gradient computed in Fig. S3B, we then plotted the magnetic force against the measured extension (dark grey circles). For reference, a simulated force-extension curve of a ~7 μmds DNA tether is shown (black squares). (**D**) When the maximum measured change in extension is known for a particular applied force, the tether's extension in nm can be converted into the number unwound base pairs since the maximum end-to-end change is proportional to the full length of the hairpin, *i.e.* 1057 bp. Since every unwound bp releases two nucleotides, this gives us directly the extension per nucleotide change. The relation between the extension-to-nucleotide conversion and the force is best approximated with a polynomial as described previously as secondary structures in the ssDNA may lead to deviations from the freely-joined chain (FJC) model [383].

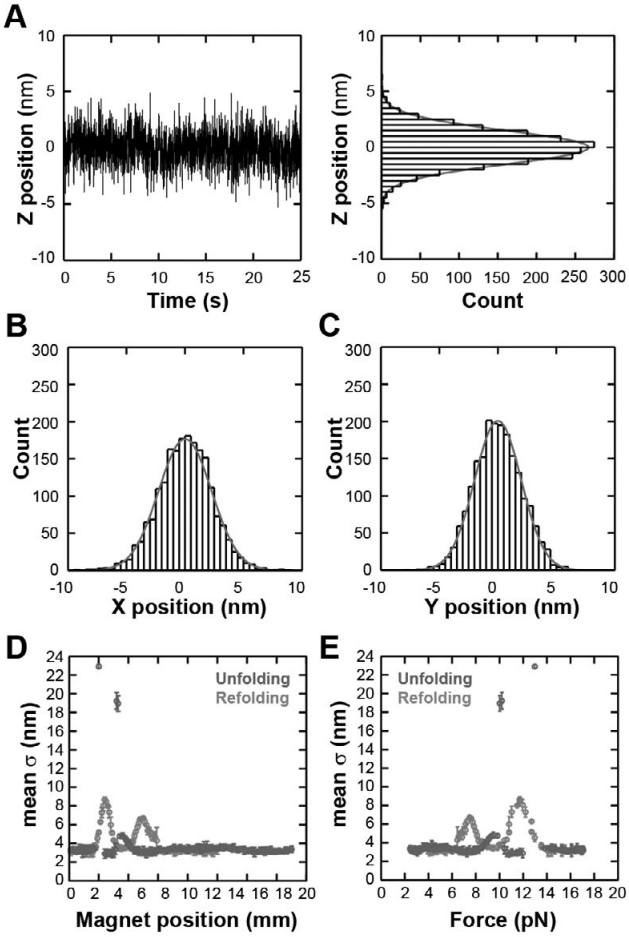

Figure S4. Tracking resolution of reference and tethered beads. (**A**) The left panel shows an example trace of the displacements of a reference bead in Z. The right panel illustrates the distribution of these displacements around the tether point '0'. A single Gaussian was fit to this distribution with a standard deviation of 1.4 nm. (**B**) Distributions of reference bead displacements in X or (**C**) Y. Single Gaussians were fit with standard deviations of 0.65 and 0.55 nm, respectively. (**D**) The tracking resolution for tethered beads plotted against the magnet position. (**E**) The tracking resolution for tethered beads plotted against the applied force.

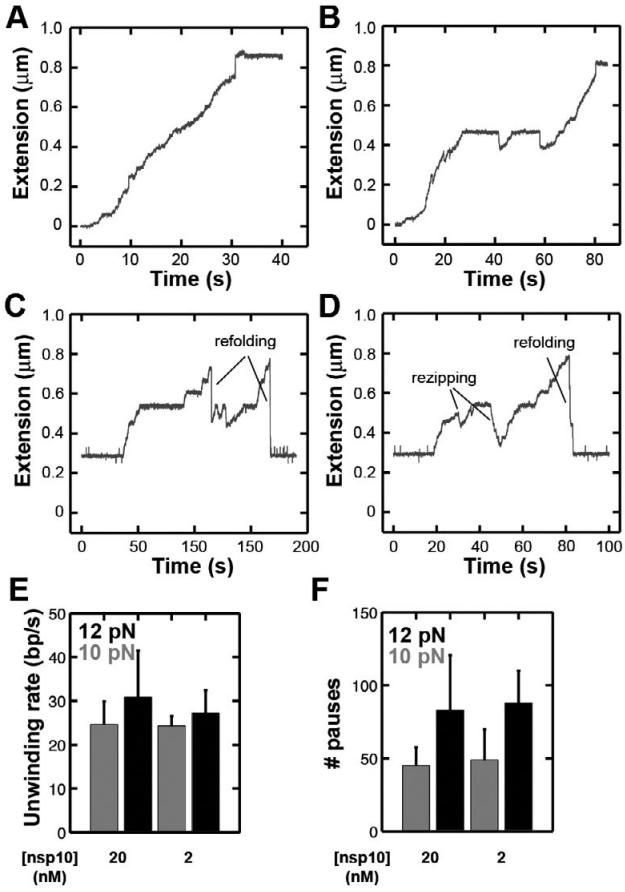

Figure S5. Variations in hairpin unwinding behaviour and refolding. (**A and B**) Although the helicase activity of EAV nsp10 predominantly resulted in the complete unwinding of the 1057-nt long hairpin, we also observed (**C and D**) events in which unwinding was abruptly terminated and the hairpin refolded (annealing of the hairpin after dissociation of the helicase or helicase back-sliding) or rezipped (hairpin closing in the wake of the helicase after template switching). All traces were observed at 2 mM ATP and 10 pN force. (**E and F**) Although we found that the unwinding velocity was dependent on the force and ATP concentration (Fig. 3), it was not dependent on the nsp10 concentration, suggesting that our measurements were performed under single-molecule conditions.

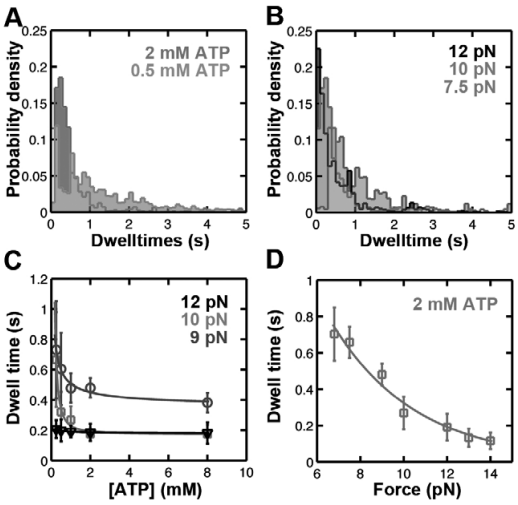

Figure S6. Dwell time analysis of EAV nsp10 at different ATP concentrations and forces. (**A**) EAV nsp10 dwell time distributions for traces obtained at 10 pN force and 2 mM ATP or 0.5 mM ATP, show that the dwell times increase with lower ATP concentrations. Bin sizes were set at 0.1 seconds. (**B**) Dwell time distributions taken at a constant ATP concentration of 2 mM show that the dwell times are also force dependent. Bin sizes were set at 0.1 second. (**C**) EAV nsp10 mean dwell times are plotted as a function of the ATP concentration and fitted with a power-law ($y = ax^b + c$). Fit values used were: 12 pN a= 0.014, b= -0.54 and c =0.17; 10 pN a = 0.056, b = -1.56, and c = 0.17; 9 pN a = 0.162, b = -0.33, and c = 0.19. (**D**) Mean dwell times are inversely correlated with the applied magnetic force. Data points from traces taken at 2 mM ATP. The dependency of the dwell times on the force can be well-fitted with a single exponential decay as shown here, or a single polynomial.

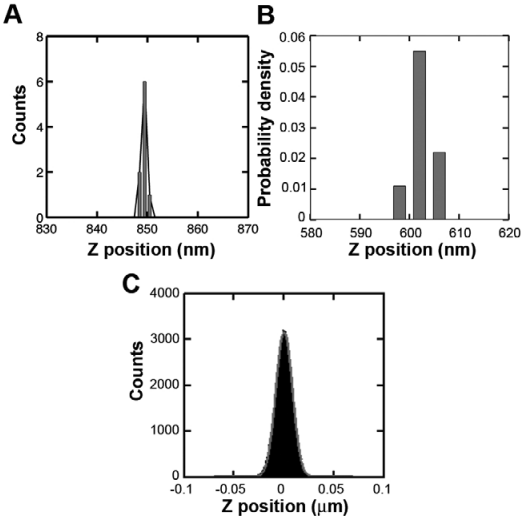

Figure S7. Alignment of helicase traces. (**A**) Alignment of the unwinding events observed on 9 different molecules shows that the standard deviation at the fully unwound position is approximately 1 nm. (**B**) Due to drift, the resolution falls along the sequence and is reduced by ~5 nm every 250 nm. (**C**) Histogram of the z-positions of a tethered bead in absence of helicase. This

trace was taken for ~ 11 minutes and the z-position distribution can be fit with a single Gaussian distribution with a standard deviation of 11 nm.

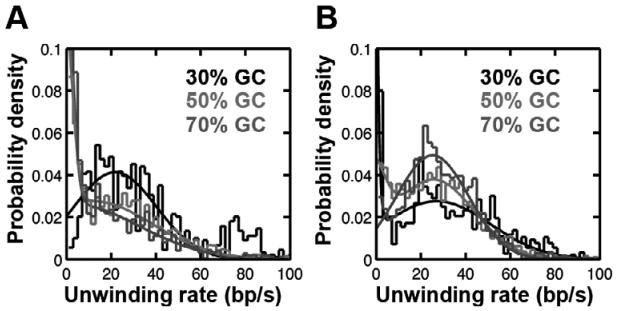

Figure S8. EAV nsp10 unwinding velocity distributions at varying GC-contents. (**A**) The unwinding velocities at 2 mM ATP or CTP (**B**) were binned according to their association with the template position and that position's GC-content. To extract the mean unwinding rate, the unwinding rates were fitted with the sum of three Gaussians. All data was taken at 10 pN force.

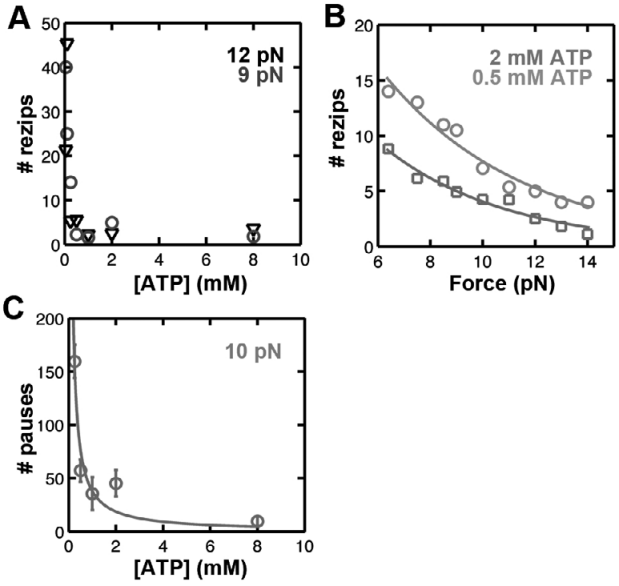

Figure S9. Rezip and pausing frequency of EAV nsp10 in the presence of ATP. (**A**) The rezipping frequency per unwinding event is dependent on the ATP concentration and (**B**) the applied force. The latter dependency can be fit with a single exponential decay. (**C**) If we keep the applied force constant and vary the ATP concentration, we also observe that the pausing frequency is dependent on [ATP]. This dependency can be fit with a single exponential decay.

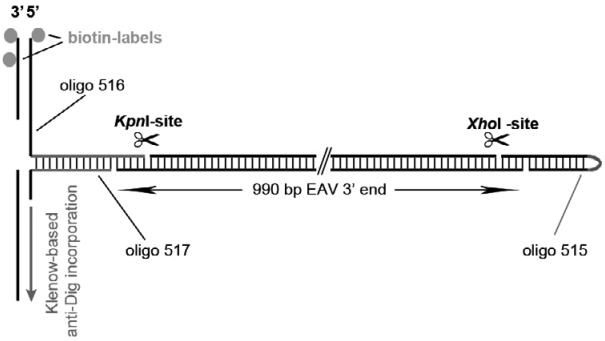

Figure S10. Construction of the 1057-kb DNA hairpin. To assemble the hairpin, the primers listed in table S1 were used in accordance to the method presented in the Material and Methods

Table S1. Oligos for hairpin construction.

Oligo	Purpose	Sequence (5′ to 3′)
E779	Cloning nsp10 fw	CATGCCATGGGCCATCACCATCACCATCACAGTGCCGTGTGCACAGTTGTGG
E789	Cloning nsp10 rv	GGATCTCGAGTTATTGCTTTTCCCAGCCACAGG
514	Fw PCR primer	TGCT**GGTACC**TACGGCAGCAAAGTCAACC
513	Rv PCR primer	AAACGACGGCCAGTGCCAAGCTCCTC
515	Hairpin loop	P-**TCGA**GAAGCGAGCGAAAGCTCGCTTC
516	5′-handle	BIO- AACCAAGTCATTCTGAGAATAGTGTATGCGG-CGACCGAGTTGCTCTTGCCTTTTT TTTTTATGCTCTT-TACAACCGGTTGACTGCTTCAGGGGTCGATCCCGCTTT-**GTAC**
	5′-handle complementary part	ACACTATTCACAGAATGACTTGGTT-BIO
517	3′-handle	P- AAAGCGGGATCGACCCCTGAAGCAGTCAACCGGTTGTA-AAGAGCATGCCAGATG GTAAGCCCTCCCGTATCGTAGTTATC-TACACGACGGGGAGTCAGGCAACTATGGATG AACGA
518	3′-handle complementary part	TGAGGCACCTATCTCAGCGATCTGTCTATTTCGTTCATC-CATAGTTGCCTGACTCCCCGT CGTGTAGATAACTACGATA-CGGGAGGGCTTACCATCTGGC